Ore Geology Reviews 92 (2018) 61–72

Contents lists available at ScienceDirect

Ore Geology Reviews

journal homepage: www.elsevier.com/locate/oregeorev

Microbial structures and possible bacterial sulfide fossils in the giant Jinding Zn-Pb deposit, Yunnan, SW-China: Insights into the genesis of Zn-Pb sulfide mineralization

Yaxiaer Yalikun[a], Chun-Ji Xue[a,*], Zhi-Jie Dai[a], Guo-Xiang Chi[b], Mostafa Fayek[c], David Symons[d]

[a] State Key Laboratory of Geological Processes and Minerals Resources, Faculty of Earth Sciences and Resources, China University of Geosciences, Xuanyuan Road 29, Beijing 100083, China
[b] Department of Geology, University of Regina, Regina, Saskatchewan S4S 0A2, Canada
[c] Department of Geological Sciences, University of Manitoba, Winnipeg, Manitoba R3T 2N2, Canada
[d] Department of Earth and Environmental Sciences, University of Windsor, ON 9 N9B3P4, Canada

ARTICLE INFO

Keywords:
Microbial sulphide structures
Bacteria sulphide fossils
FESEM and EPS
SIMS in situ S-isotopic micro-analysis
Jinding Pb-Zn deposit
SW-China

ABSTRACT

The Jinding Zn-Pb sulfide deposit, Lanping, Yunnan, China, is one of the youngest sediment-hosted giant Zn-Pb deposit in the world. It is also a well known deposit in China. The large scale of the mineralization and especially the huge volume of H_2S that was required to precipitate the Zn-Pb sulfide are of great interest to ore geologists. Ore microscopy shows microbial structures such as framboidal sphalerite, spherical aggregates of galena-sphalerite, oolite sphalerite, dendritic colloidal sphalerite-pyrite, metacolloidal sphalerite-pyrite, multinuclear-metacolloidalring-like sphalerite-pyrite, botryoidal sphalerite-pyrite, framboidal pyrite and bacterial plate-like of galena-sphalerite. Detailed observations and analyses of the microbial structures at micron to nanometer scales by field emission scanning electron microscopy (FESEM) and energy dispersive spectrometry (EDS) reveal that the bacteria fossils are composed of sphalerite, galena or pyrite or of multiple sulfide minerals with calcite and that they are distributed in bacterial colonies in the ore. The individual bacteria fossils are spherical, botryoidal or ring-like with a diameter of 200–500 nm. Filamentous, mucoid and tubular extracellular polymeric substances (EPS) are commonly observed that are closely associated with, and have the same composition as, the bacteria fossils. Secondary ion microprobe analysis (SIMS) by in situ sulfur micro-isotopic analysis of the microbial sulfide structures and bacteria fossils yield $\delta^{34}S_{V\text{-}CDT}$ values varying from −48.6 to −9.5 per mil, indicating that there was a high percentage of sulfate reducing bacteria in the Zn-Pb sulfide mineralization process. Previous analyses have shown that the Zn-Pb mineralization was formed at a shallow depth and low temperature with barely visible hydrothermal alteration, the presence of evaporitic sulfate layers and paleo-oil reservoir characteristics. The authors believe that bacterial sulfate reduction might be the key H_2S production mechanism in the Jinding dome that was required to form this giant Pb-Zn sulfide ore body.

1. Introduction

Bacteria may play an important role in the mineralization of sediment-hosted base metal and uranium deposits (Southam and Saunders, 2005), and sulfate-reducing bacteria (SRB) may be one of the key factors required for generation of the H_2S required to precipitate the mineralization (Gustafson and Williams, 1981; Bechtel et al., 1996, 1998; Warren, 2000; Labrenz et al., 2000; Watson et al., 2000; Kyle and Li, 2002; Marshall et al., 2004; Southam and Saunders, 2005; Xue et al., 2007a, 2015; Tang et al., 2014). Bacterial fossils have been found in sandstone-hosted uranium ores (Min et al., 2005; Cai et al., 2007) and SRB have played a key role in the precipitation of the uranium minerals. However, the presence of SRB has not been directly shown in the sediment-hosted lead, zinc, copper or other base metals deposits.

The Jinding deposit near Lanping, Yunnan currently has Pb-Zn reserves of > 10 Mt, and it is also one of the youngest sediment-hosted giant Zn-Pb deposit (Xue et al., 2003, 2007a, 2015). A recent palaeomagetic dating study of this deposit gave a 23 ± 3 Ma mineralization age (Yaxiaer et al., 2017). More than 22 Mt of lead and zinc metals were precipitated in the small 8 km^2 Jinding ore field (Zhu et al., 2000). From this tonnage, it is inferred that 3.17×10^6 m^3 of H_2S was required to create the Zn-Pb mineralization (Gao et al., 2008a). The required H_2S is actually much greater because Jinding also contains a large FeS_2 deposit (Xue et al., 2003). How were such huge volumes of H_2S

* Corresponding author.
E-mail address: chunji.xue@cugb.edu.cn (C.-J. Xue).

https://doi.org/10.1016/j.oregeorev.2017.11.004
Received 25 February 2017; Received in revised form 31 October 2017; Accepted 6 November 2017
Available online 07 November 2017

generated to participate in the mineralizing process? Many layers of gypsum and salt occur in the host Lanping basin so that either thermochemical sulfate reduction (TSR) or bacterial sulfate reduction (BSR) could have been the main mechanism of H_2S generation (Shi et al., 1983; Bai et al., 1985; Yin et al., 1990; Chen, 1991, 1992; Zhou and Zhou, 1992; Xue et al., 2003, 2007a). It has also been suggested that organic matter was an important reducing agent that caused sulfate reduction to create H_2S according to organic petrography and geochemistry studies that indicate the Jinding ore field was an oil and gas paleoreservoir (Xue et al., 2007a,b, 2009, 2010; Gao et al., 2008a,b). From previous research on the ore-forming process and ore S-isotopic compositions, the H_2S required for the main stage of Zn-Pb sulfide mineralization had been thought to be TSR generated, although there is evidence that a BSR event might have occured in the Jinding dome before the major stage of Zn-Pb sulfide mineralization (Xue et al., 2007a, 2010; Gao et al., 2008b). Conversely, it has also been suggested that the H_2S required to precipitate the main Zn-Pb orebody was BSR rather than TSR generated (Tang et al., 2014). Further it is not clear whether BSR occurred at the mineralization site or elsewhere with the H_2S migrating into the dome, although the BSR generated H_2S is generally confirmed to be present in the Jinding sulfide mineralization. Recent ore fabrics and related in situ micro-sulfur isotopic research have shown that the BSR processes occurred at the metallization site rather than elsewhere (Xue et al., 2015). However, there has been no previous report of microbial structures and bacteria fossils in the Zn-Pb sulfides.

To better constrain our understanding of the TSR-BSR problem at Jinding, the Zn-Pb sulfide ores in the main orebody have been examined by ore microscopy. In this paper we report on the morphology and composition of the sulfide minerals that have been observed and analyzed on a micro- to nanometer scale using a field emission scanning electron microscope (FESEM) and energy dispersive spectrometer (EDS). Finally, the in situ S-isotopic compositions of the sulfide minerals in the microfabrics have been analyzed using secondary ion microprobe (SIMS) analysis.

2. Regional geological setting

The Jinding Zn-Pb deposit is located in the northern part of the Lanping-Simao basin (Fig. 1a). The basin is between the Tibet-Yunnan plate to the west across the Lancangjiang suture zone and the Yangtze plate to the east across the Jinshajiang-Ailaoshan suture zone. The basin trends NNW with a length of about 400 km and a width of about 150 km (Xue et al., 2004). From the analysis of the tectonics, magmatics and infilling sedimentary strata, it can be summarised that the basin was a microcontinent in the Proto-Tethys Ocean from the Proterozoic to the early Paleozoic. The Proterozoic rocks consist of schist, gneiss, marble and high-grade metamorphosed volcanics that formed in uplifted zones along both sides of the basin. The Lower Paleozoic flysch is composed of low-grade metamorphosed clastic rocks with argillaceous carbonate interlayers, and it is partially exposed in some small uplifts in the basin and at its margin. The region developed into a stable block as the Proto-Tethys Ocean closed at the end of the Caledonian orogeny before a Silurian hiatus. As the Paleo-Tethys Ocean opened along the Lancangjiang and Jinshajiang-Ailaoshan fault zones during the Early Devonian to Early Carboniferous, the basin became a microplate between the Yangtze and Tibet-Yunnan plates, as the flysch formations were deposited in the ocean around the basin's margins. Volcanic arcs developed along both sides of the microplate due to Permian subduction. As the Paleo-Tethys Ocean closed at the end of the Permian, the microplate became entrapped between the Yangtze and Tibet-Yunnan plates as part of Laurasia (Xue et al., 2002a, 2004).

The Lanping-Simao basin records the only continental environment during the Mesozoic and Cenozoic periods. Regionally, it existed as a rift basin in the Triassic, a depression basin in the Jurassic-Cretaceous and a strike-slip pull-apart basin in the Cenozoic. After the release of regional compressional stress from the closure of the Paleo-Tethys Ocean, the ensuing Lower Triassic hiatus and regional uplift established an extensional setting in the basin. The extension caused Middle Triassic rifting along the Jinshajiang-Ailaoshan and Lancangjiang fault zones. Regionally the Middle-Upper Triassic rocks consist of clastic and carbonate rocks of marine and marine-terrestrial transitional facies with a large volume of the felsic-mafic bimodal volcanic rocks that are characteristic of continental rifts. Near at the end of the Triassic, the Nujiang Ocean opened with a NS-trend to the west of the region and pushed eastward, which gradually uplifted the basin's western margin and caused an intracontinental depression of the region. During the Jurassic-Cretaceous, the Nujiang Ocean closed, perhaps because of the rapid expansion of the Yarlung-Zangbo River Ocean, to create the Lanping-Simao basin, which was infilled with terrestrial clastic rocks from the adjacent uplifts. Toward the end of the Cretaceous, the Yarlung-Zangbo River Ocean closed as the northern side of the Indian plate collided with the Eurasian plate. The collision uplifted the basinal region again, resulting in an unconformity surface between the Upper Cretaceous and Paleocene strata. During the Paleogene, the continued transpression between the Indian and Eurasian plates caused NNW-trending strike-slip faults to be strongly developed along the northeast margin of the Qinghai-Tibet plateau. The collision also caused the Lanping-Simao strike-slip pull-apart basin to be formed and filled with red clastic and evaporite strata. The continued docking and intense compression between the Indian and Eurasian plates led to widespread large-scale thrust faulting in the region, resulting in the Mesozoic strata being often thrust over the Paleogene formations. The Neogene formations consist of trachytic clastic volcanic and red sandstones (Xue et al., 2002a, 2004). The basin is characterized by fault-block uplift during the Quaternary.

Within the Lanping basin, mantle-derived Cenozoic alkalic intrusions crop out at Yongping, Weishan and other locations (Yin et al., 1990; Lü and Qian, 1999). Several Cenozoic structural domes such as the Jinding dome (Xue et al., 2007c) and Cenozoic metamorphic belts like the Wuliangshan belt (YBGMR, 1990) formed along the main NNW-trending fault within the basin. All of these features might be related to Himalayan uplift and related upwelling thermal flux. The Jinding ore field basin also hosts a large evaporite sedimentary gypsum deposit, other sediment-hosted silver, copper, zinc and lead deposits such as the Baiyangping (Xue et al., 2002a, 2003) and Jinman deposits (Chi and Xue, 2011), and the large Hexi celestite deposit (Xue et al., 2002b; Hu et al., 2013). The processes of the basin sedimentation, thrust faulting and the structural doming were important geological steps in the Cenozoic formation of the huge Jinding Zn-Pb deposit (Xue et al., 2002a, 2004).

3. Ore geology

Upper Triassic, Middle Jurassic, Cretaceous, Paleocene and Eocene rocks are exposed in the Jinding Zn-Pb ore field (Fig. 1). The Upper Triassic, from oldest to youngest, includes: the Sanhedong Formation composed of limestone, marlstone, bitumen-rich limestone and argillaceous dolomite; the Waluba Formation composed of mudstone and siltstone; and the Maichuqing Formation composed of gray black carbonaceous argillite, siltstone and sandy mudstone. The Middle Jurassic system is represented by the Huakaizuo Formation and composed of purple siltstone and mudstone. The Lower Cretaceous Jingxing Formation contains light gray quartz sandstone. The Upper Cretaceous lithologies include the older Nanxin Formation which includes purple medium-coarse grained sandstone and mudstone interbeds, and the younger Hutousi Formation that is composed of light gray feldspar-quartz sandstone. The Paleocene Yunlong Formation has a lower member consisting of silty mudstone and an upper member of conglomerate-bearing sandstone, sandstone and gypsiferous argillaceous siltstone. Above it is the Eocene Guolang Formation that is composed of quartz sandstone.

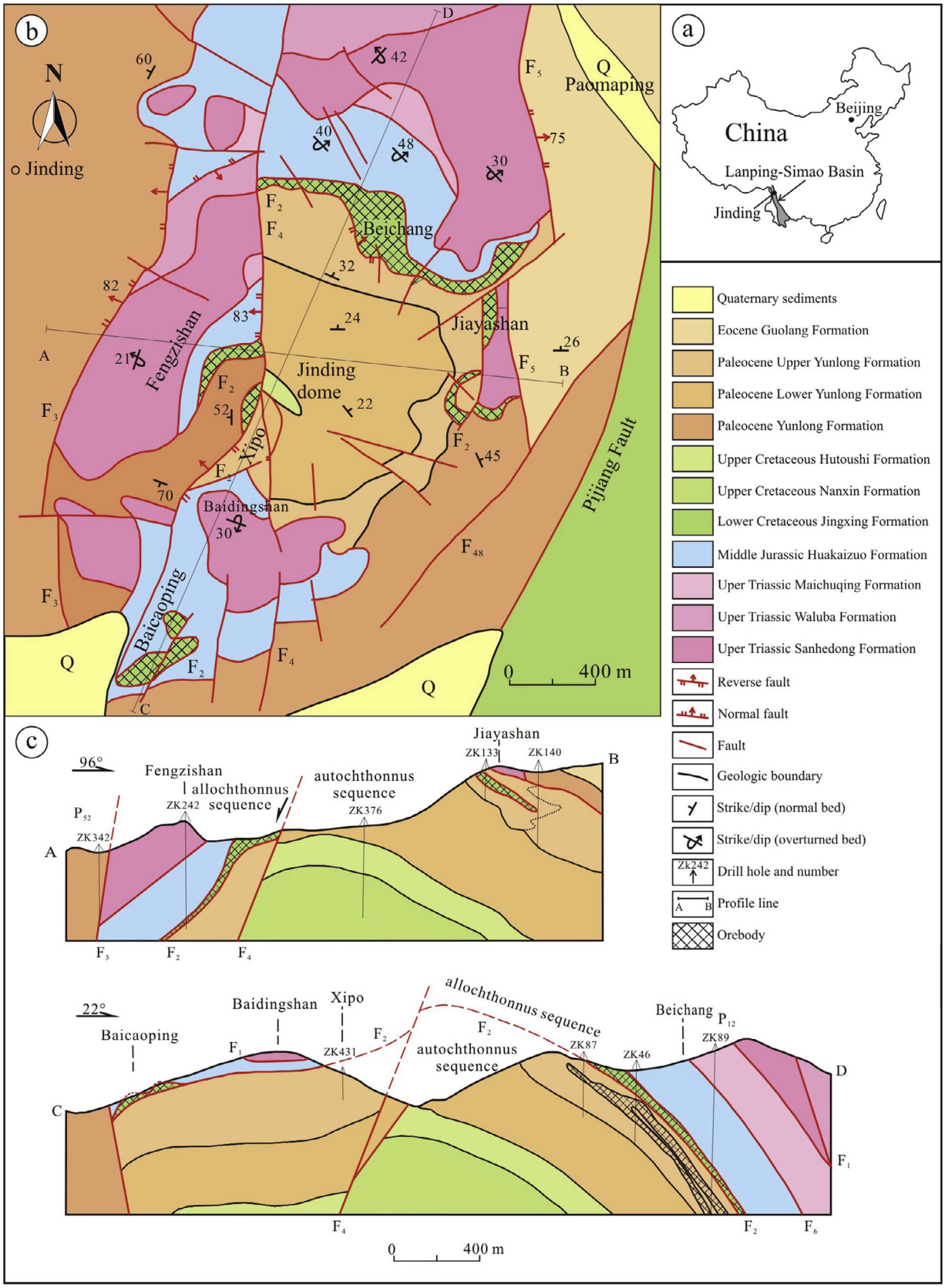

Fig. 1. Geological map and sections of the Jinding Zn–Pb deposit (modified from Xue et al., 2015).

The Jinding Zn-Pb sulfide orebodies are hosted in the Lower Cretaceous Jingxing Formation and the upper part of the Paleocene Yunlong Formation (Fig. 1) The lithology of Yunlong Formation consists of conglomerate on the eastern side of the ore field that grades to gravel-bearing quartz sandstone and sandstone on the western side.

After the sedimentation of the Jinding strata, a NE-SWward thrust

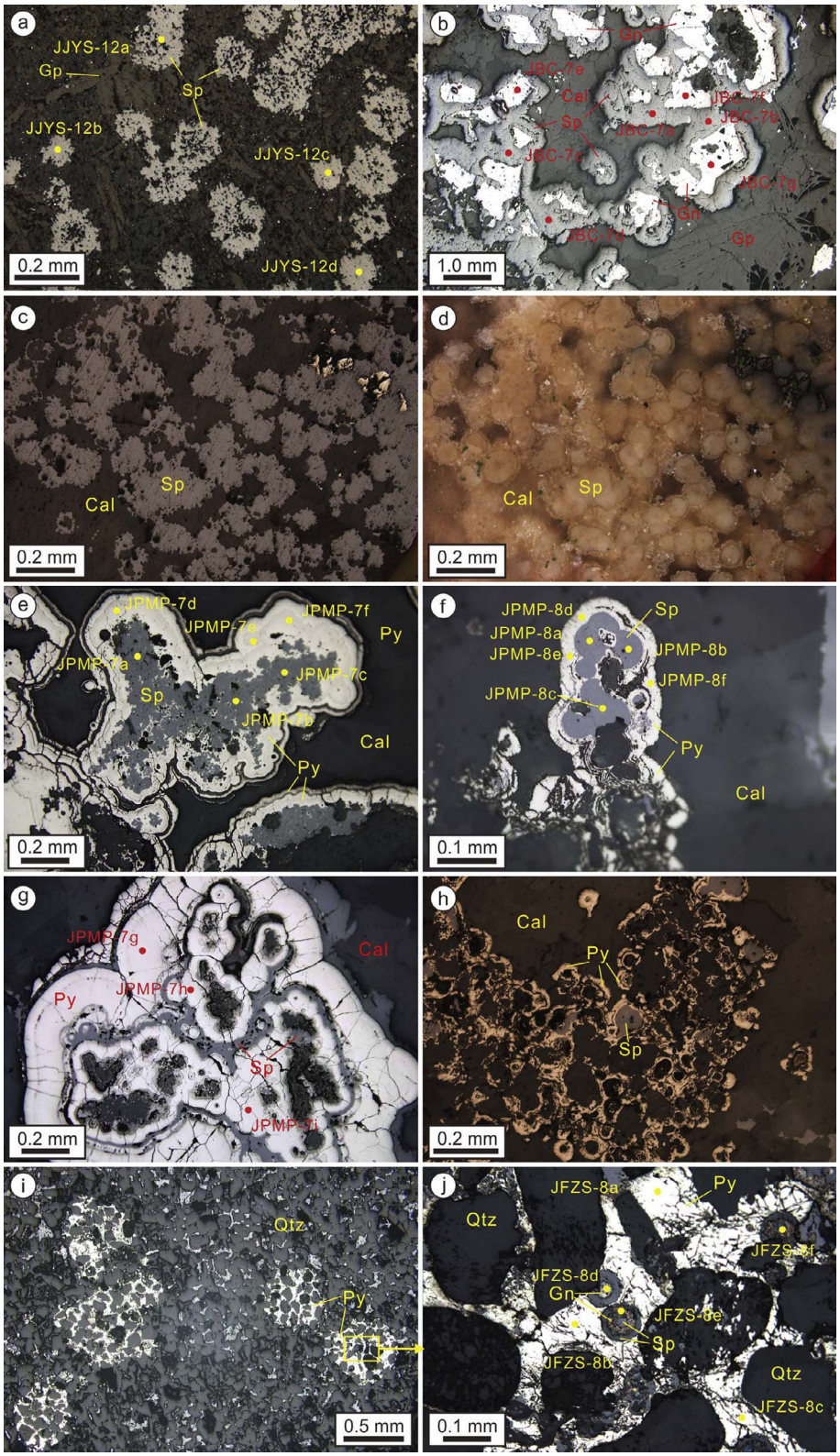

Fig. 2. Photomicrographs of bacterial structures and textures in the Jinding lead–zinc ore. The samples come from ore in either conglomeratic sandstone of the Jiayashan (JJYS) or Paomaping (JPMP) segments or sandstone of the Beichang (JBC) or Fengzishan (JFZS) segments of the Jinding ore field. All samples are from the SIMS sites listed in Table 1. a. Framboidal sphalerite is an assemblage of microcrystalline sphalerite that is globular in shape and has an irregular margin with a jagged edge. The framboids are 0.05–0.1 mm in diameter and contain internal quartz debris (sample JJYS-12, reflected plane-polarized light (rppl)). b. The spheroidal aggregates contain a core of subhedral galena crystals that is rimmed by colloidal sphalerite. The spheroids are assembled into a globular structure with a smooth edge and a 0.5–2.0 mm diameter (sample JBC-7, rppl). c. Oolite-like sphalerite and "raspberry"-shaped sphalerite are linked to each other. Single roe eggs and "raspberries" of sphalerite have a diameter 0.05–0.1 mm (sample number, JBC-17, reflex polarized). d. Photomicrograph of c under reflected cross-polarized light; e. Dendritic colloidal sphalerite-pyrite in which the central colloidal sphalerite is surrounded by colloidal pyrite to form a globular morphology (sample number JPMP-7, reflex polarized). f. Metacolloidal sphalerite-pyrite in which the metacolloidal pyrite surrounds the metacolloidal sphalerite (sample number JPMP-8, reflex polarized). g. Multinuclear-metacolloidal-ring-like sphalerite-pyrite in which there are irregular "cores" composed of nonuniform carbon-mud aggregate surrounded by sphalerite. The multiple "cores" are in turn surrounded by an envelope of pyrite (sample number JPMP-7, reflection single polarizing). h. Botryoidal sphalerite-pyrite in which the sphalerite-pyrite aggregates are linked to each other to form grape-shaped clusters (sample number JPMP-8, reflex polarized). i. Framboidal sphalerite in unevenly distributed patches of pyrite. Individual spheroids are 0.2–0.6 mm in diameter (sample number JFZS-8, reflex polarized). j. Magnification of the yellow rectangle in i to show a bacterial plate-like galena-sphalerite between quartz grains. The plate has a zonal structure and spherical shapes that contain a core composed mainly of sphalerite or galena. (sample number JFZS-8, reflected polarized light).

fault occured including the main F_2 fault (Fig.1b) and some other minor thrust faults such as F_1 and F_6 (Fig. 1c) (Xue et al., 2003, 2007a). The attitude of the autochthonous system is normal and consists of the Upper Cretaceous Nanxin, Hutousi and the Paleocene Yunlong formations from bottom to top. Conversely the allochthonous system is overturned with the Lower Cretaceous Jingxing Formation, the Middle Jurassic Huakaizuo Formation, the Upper Triassic Maichuqing and Sanhedong formations (Xue et al., 2007c). Thereafter the thrust structure was deformed by local doming into the Jinding ore field. Thus the core of the Jinding dome is composed mainly of rocks of the autochthonous system, whereas the dome's flanks are composed of allochthonous rocks (Fig. 1b and c).

The Jinding Zn-Pb orebodies are hosted in the hanging wall the Jingxing formation, and also in the footwall the upper member of the

Yunlong Formation. The boundaries are all gradational between the ore zones and the wall rock and the related wall-rock alteration. The Jinding Zn-Pb sulfide mineralization was likely emplaced either late in, or after the end of, the doming process (Xue et al., 2007c). After mineralization, the Jinding dome cracked to create a number of faults that radiate away from its core and cut the strata, thrust structures and ore-bodies. Thus the original continuous ore-bodies were divided into the Beichang, Fengzishan, Nanchang, Jiayashan, Paomaping and other ore zones of the Jinding ore field (Fig. 1b). The youngest NS-trending faults, such as the F_3, F_4 and F_5 faults, resulted in further uplift and erosion throughout the ore field.

The Zn-Pb sulfide ore in the Jinding Formation is hosted in sandstone, whereas the ore in the Yunlong Formation is hosted in both conglomerate-bearing sandstone and sandstone. The main ore minerals are sphalerite and galena with subordinate pyrite and rare chalcopyrite. Ore microscopy shows that the sulfide minerals mostly replaced calcite cement and partially quartz, plagioclase, limestone gravel and other clastics in the clastic sedimentary rocks. Most of the sulfide minerals show allotriomorphic crystallinity (50–100 μm), colloform textures and disseminated taxitic and framboidal structures. The average ore grade is 6.1% Zn and 1.3% Pb (YBGMR, 1990; Xue et al., 2003, 2007a).

4. Samples and methods

The studied samples were collected from the Beichang and Jiayashan open pits and from tunnels in the Fengzishan and Paomaping mines. All of the samples are from freshly-mined ore faces. Double-sided polished thin sections were prepared for observation and analysis from six locations, ie the Beichang (JBC-7 and JBC-17), Jiayashan (JJYS-12), Fengzishan (FZS-8) and Paomaping (JPMP-7 and JPMP-8) ore zones.

The double-sided polished thin sections were examined first under a polarizing microscope using both transmitted and reflected light to select sulfide minerals for further field emission scanning electron microscopy (FESEM) observation, energy dispersive spectrometry (EDS) detection and micro-in-situ sulfur isotopic analysis. The in-situ sulfur isotopic compositions of the sulfide micro-structures were analyzed using a secondary ion microprobe spectrometer (SIMS) on a CAMECA IMS-7F ion microprobe at the University of Manitoba. The instrumental analytic methods, processes and conditions follow those described by Xue et al. (2015). The standard materials used for the SIMS analysis were massive coarse-grained, homogeneous sulfide minerals from the Balmat mine, New York, USA, that include pyrite ($\delta^{34}S = +15.1‰ \pm 0.3‰$), sphalerite ($\delta^{34}S = +14.0‰ \pm 0.3‰$) and galena ($\delta^{34}S = +15.6‰ \pm 0.3‰$). The results are stated relative to the Vienna-Canyon Diablo Troilite (VCDT) standard with an analytical error of 0.4‰. The FESEM observations and EDS were done at the State Key Laboratory of Geological Processes and Mineral Resources of the China University of Geosciences. The instrument used was a SU-PRATM-55 electron microscope with a corollary Oxford EDS. The accelerating voltage was 10 kv with a working distance of 8.7–15.0 mm.

5. Results

5.1. Morphological structures

Many styles of sulfide ore structures have been observed using a polarizing microscope under reflected light. They include framboidal sphalerite (Fig. 2a), spherical aggregates of galena-sphalerite (Figs. 2b, Fig. 3a), oolite sphalerite (Fig. 2c and d), dendritic colloidal sphalerite-pyrite (Fig. 2e), metacolloidal sphalerite-pyrite (Fig. 2f), multinuclear-metacolloidal ring-like sphalerite-pyrite (Fig. 2g), botryoidal sphalerite-pyrite (Fig. 2h), framboidal pyrite (Fig. 2i) and bacterial plate-like of galena-sphalerite (Fig. 2j).

Framboidal sphalerite is frequently observed in the sandstone-hosted Zn-Pb sulfide ore. The structure consists of microcrystalline sphalerite that is aggregated into a spherical shape with irregular serrated edges about 0.05–0.1 mm in diameter and contains internal quartz debris (Fig. 2a).

Spherical aggregate of galena-sphalerite is frequently formed in the conglomerate-bearing sandstone-hosted Zn-Pb sulfide ore. Its core is a subeuhedral crystal of galena surrounded by colloidal sphalerite. The aggregate is globular or irregularly globular in shape with a smooth edge that is 0.5–2.0 mm in diameter (Fig. 2b).

Oolite sphalerite is commonly seen in the sandstone-hosted Zn-Pb sulfide ore. This spherical aggregate is oolite-like in shape with a taxitic structure, which have gathered into crowded groups with links to each other (Fig. 2c). This structure is best observed by microscope under reflected cross-polarized light (Fig. 2d). A single sphalerite “spawn” is 0.05–0.1 mm in diameter.

Dendritic colloidal sphalerite-pyrite is often observed in the conglomerate-bearing sandstone-hosted Zn-Pb ore. It occurs in inhomogeneous clusters and groups. The colloidal pyrite is usually formed around an irregular aggregate of colloidal sphalerite. Overall the shape looks dendritic (Fig. 2e). Also there are bacterial plate-like structures in the colloidal pyrite (Fig. 5a).

Metacolloidal sphalerite-pyrite is frequently observed in the conglomerate-bearing sandstone-hosted Zn-Pb ore and also occurs in inhomogeneous clusters and groups. The metacolloidal spherical sphalerite core is often surrounded by metacolloidal pyrite. The whole aggregate is globular in shape (Fig. 2f).

Multinuclear-metacolloidal ring-like sphalerite-pyrite is commonly found in the conglomerate-bearing sandstone-hosted Zn-Pb ore. The ring-like metacolloidal-pyrite and/or -sphalerite has an irregular concentricity with a number of irregular cores composed of nonuniform carbon-mud aggregate (Figs. 2g, 4). The colloidal pyrite rings are often wider than the colloidal sphalerite rings. Radial fractures in the metacolloidal component are commonly observed (Fig. 2g).

Botryoidal sphalerite-pyrite is often observed in the conglomerate-bearing sandstone-hosted Zn-Pb ore as inhomogeneous clusters and groups. The structure occurs in spherical aggregates that are composed of nuclear cores of colloidal sphalerite with a surrounding colloidal pyrite ring. The aggregates are linked to each other to form clustered groups like grape clusters (Fig. 2h). Also a calcite bacterial plate is observed between the spherical aggregates (Fig. 6).

Framboidal pyrite is often seen in the sandstone-hosted Zn-Pb as inhomogeneous intergranular clusters and groups. A single pyrite framboid with quartz fragments is 0.2–0.6 mm in diameter. There is a bacterial plate-like galena-sphalerite that has a zonal structure and spherical shape of 0.05–0.08 mm in diameter with a core composed mainly of sphalerite or galena. The core’s inner zone is galena and its outer zone is sphalerite within the pyrite rim (Fig. 2j). The sphalerite zone in the structure may or may not be continuous (Fig. 3a).

5.2. Measured properties

The results for the SIMS in situ S-isotopic analysis of the sulfide minerals described above are listed in Table 1. The numbers for the analysis spots listed in Table 1 correspond to those shown in Fig. 2.

The microbial structures and bacteria fossils (Figs. 3–6) consist of paragenetic sphalerite, galena, pyrite and calcite that have been observed and detected by FESEM and EDS at the micron or nanometer scale. The bacterial plate structure of galena-sphalerite (Fig. 2j) exhibits multiple plates that are linked to each other in clusters and look exactly like bacteria (Fig. 3a). FESEM shows that the aggregates consist of galena cores surrounded by zoned galena-sphalerite rings. The galena cores are from 20 to 80 μm in diameter with a rough surface (Fig. 3b). The zoned sphalerite ring is frequently discontinuous and also has a rough surface from the aggregation of multiple fine grains (Fig. 3c). EDS detection demonstrates that the ring is composed of sphalerite (Fig. 3e). The individual bacteria fossils of sphalerite are round in shape and about 200 nm in diameter (Fig. 3d) and they are linked together in

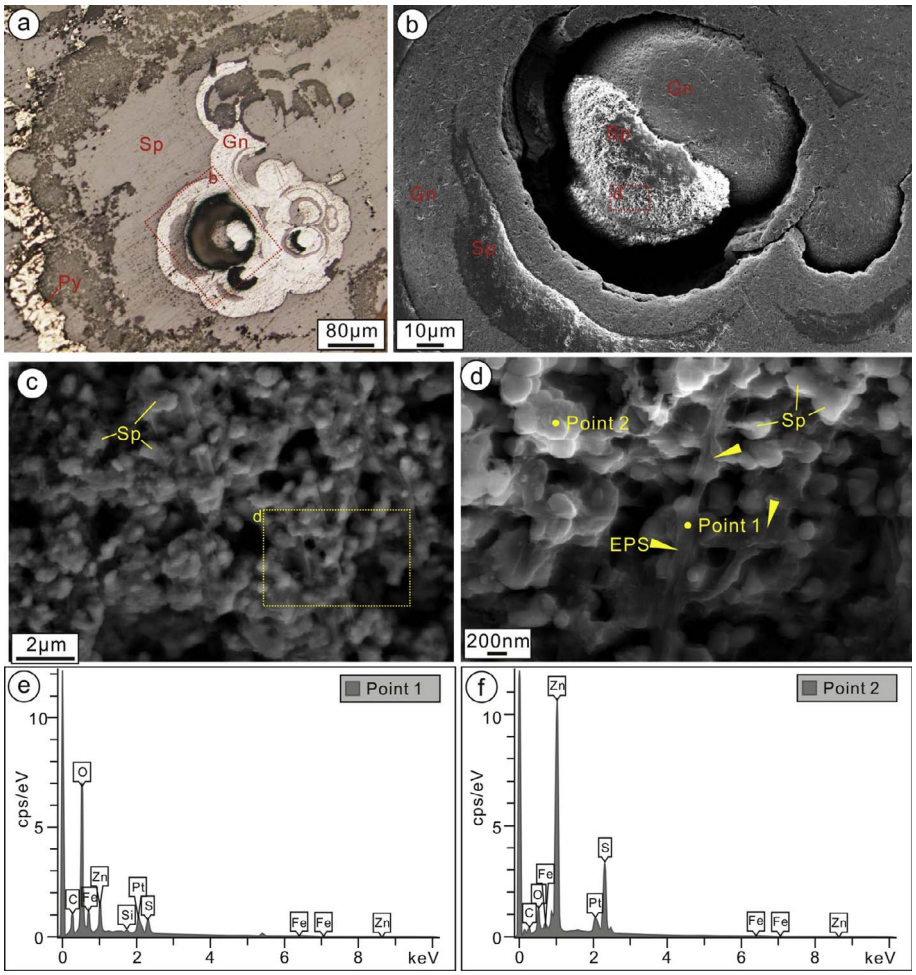

Fig. 3. FESEM photos and the results of energy distribution spectrum (EDS) analysis of bacteria fossils from plate galena-sphalerite. a. Magnification of part of Fig. 2i showing plate-galena and sphalerite; b. Further magnification of a; c. Magnification of part in b showing nano-balls connected by protonema of sphalerite; d. Magnification of part in b showing nano-balls connected by protonema of sphalerite; e. EDS analysis results for spot 1 from d; f. EDS analysis results for spot 2 from d; Sp-Sphalerite, Gn-Galena, Py-Pyrite, EPS- Extracellular polymers.

clusters. A filamentous or mucoid mineral is also observed that links the fossils (Fig. 3c and d), which EDS identifies as sphalerite (Fig. 3f).

Spherical bacteria fossils of micron scale are crowded into clusters (Fig. 4a–c) and have been observed in the multinuclear-metacolloidal-ring-like sphalerite-pyrite structure (Fig. 2g) by FESEM. The fossils are shown by EDS to be composed of pyrite and sphalerite (Fig. 4d and e). A pyrite aggregate often forms the core of the fossil with a sphalerite aggregate forming a ring zone around it. The pyrite core is spherical in shape with a rough surface, and it is composed of many more bacteria fossil grains of fine pyrite. The sphalerite in the outer zone shows similar structural characteristics (Fig. 4c–e).

Colloidal pyrite is frequently observed in Jinding's conglomerate-bearing sandstone-hosted Zn-Pb sulfide ores. The pyrite exhibits a spheroidal granular texture and a concentric structure with a diameter of 20–40 μm (Fig. 5a). The micron to nanometer scale of the bacteria fossils is seen by FESEM in the core of the colloidal pyrite spherical aggregate (Fig. 5b). The fossils are spherical grains that are linked to each other in clusters (Fig. 5b and c). A mucoid filamentous material can be seen between the nanometer-sized grains of bacteria fossils by FESEM (Fig. 5c). EDS detection confirms that the fossils are composed of pyrite (Fig. 5d).

A bacteria fossil aggregate that is seen by FESEM and composed of micron to nanometer-sized calcite grains co-exists with the meta-colloidal pyrite in the conglomerate-bearing sandstone-hosted Zn-Pb sulfide ores (Fig. 6a–c). The aggregate is spheroidal in shape with a diameter of about 10 μm and it is found in dense clusters of other calcite fossils of similar size (Fig. 6b). The individual bacteria fossils are shown to be composed of calcite by EDS detection (Fig. 6d).

6. Discussion

Pyrite framboids or other micro-organism microstructures such as fossil bacteria can be difficult to identify in the geological record because of either the recrystallization of minerals such as pyrite, sphalerite and calcite or the influence of late-stage mineral replacement (Scott et al., 2009; Wacey et al., 2015). However, we can observe the morphology and size and analyze the elemental composition of microstructures produced by such micro-organisms and bacteria fossils using FESEM and EDS methods (Rickard and Zweifel, 1975). When these methods are combined with the $\delta^{34}S$ data, we can better understand whether or not the microstructures are related to bacteria (Kohn et al., 1998).

6.1. Bacteriogenic structures, bacteria fossils and sulfate-reducing bacteria

In the Jinding Pb-Zn sulfide ore beds are found a variety of special types of sulfide. They include framboidal and oolite-like sphalerite in monomers of "core – coating" binary structures. Their morphology and composition are similar to framboidal sphalerite found in the Ulagen and Bleiberg Pb-Zn deposits (Kucha et al., 2005; Xue et al., 2014). The formation of both structures is associated with SRB.

At Jinding the galena and sphalerite form globular clusters with galena as the core and colloidal sphalerite as the surrounding coating. Colloidal sphalerite-pyrite and metacolloidal sphalerite-pyrite crystallites have sphalerite as the core and colloidal or metacolloidal pyrite as the surrounding coating. Also, in multiple nuclear-metacolloidal and ring-like sphalerite-pyrite structures, we found sphalerite as the core with carbon as the surrounding coating. We believe they might also

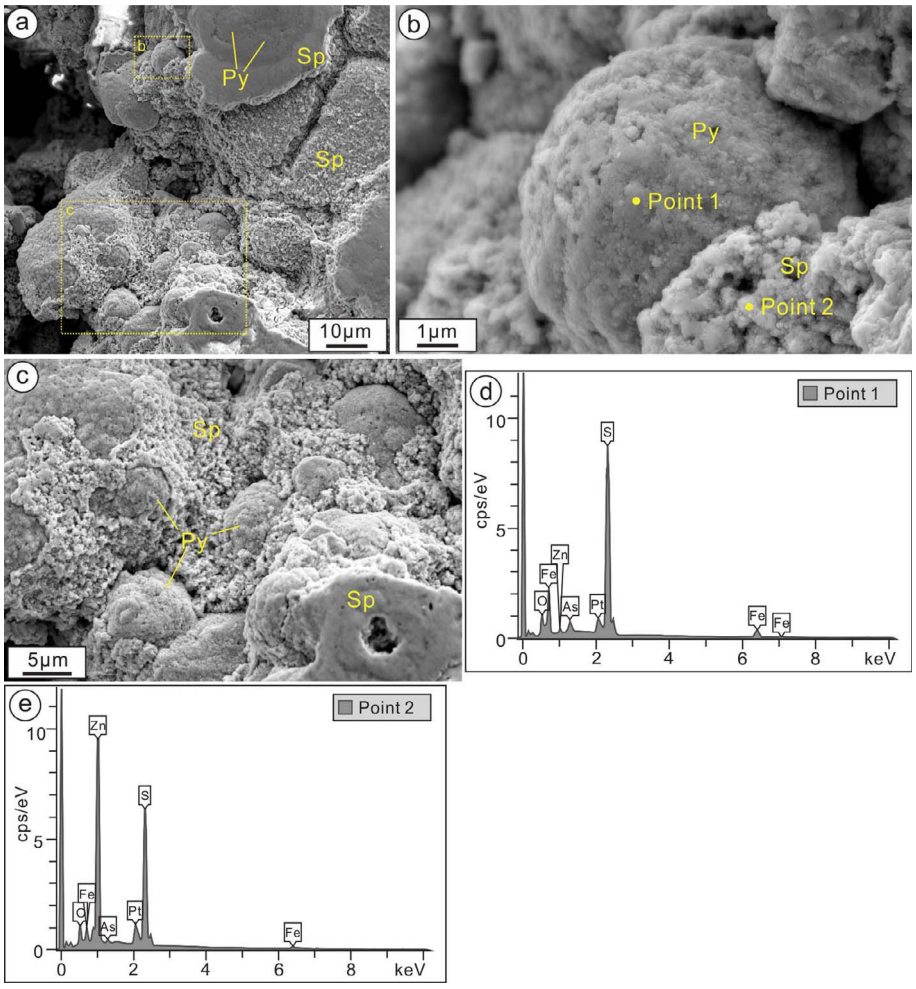

Fig. 4. FESEM photos and the results of EDS analyses for bacteria fossils from multi-core gelatinous pyrite, sphalerite. a. Large group of micron-scale bacteria fossils composed of pyrite and sphalerite in multistructures; b. Magnification of a showing the assembly of the pyrite core; c. Magnification of a showing enlargement of the bacteria fossils; d. EDS analysis of spot 1 in c; e. EDS analysis of spot 2 in c. Sp-Sphalerite, Py-Pyrite.

formed by bacterial activity.

Sphalerite-pyrite botryoides are connected to each other in multiple colloidal pyrite-sphalerite globular groups like grapes with each unit having a “core – coating” binary structure in which the core is composed of sphalerite or calcite and the surrounding coating is pyrite. These globular clusters are similar to those found in the Navan Pb-Zn deposit of Ireland (Bawden et al., 2003).

Framboidal pyrite is commonly found in a sedimentary environment and is considered to be the result of microbial activity. The structural layering of the galena and sphalerite crystallites in the Jinding deposit

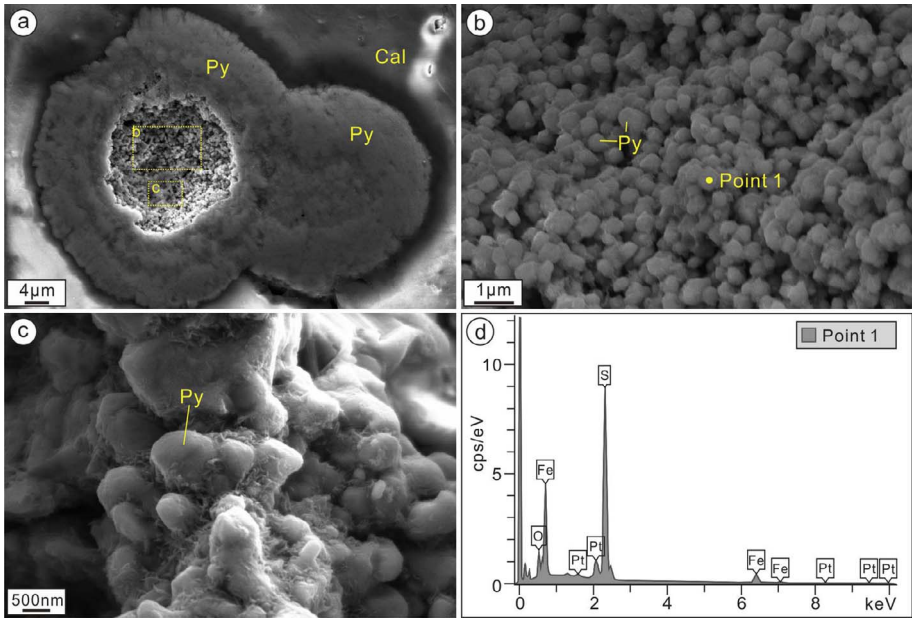

Fig. 5. FESEM photos and EDS analyses of bacteria fossils from colloidal pyrite. a. Colloidal pyrite in the Zn-Pb ore is characterized by orbicular and concentric ring structures; b. Increased magnification of a showing the submicron scale of the bacteria fossils; c. Further magnification of a showing pyrite bacteria fossil at a nanoscale; d. EDS analysis of spot 1 in b. Py-pyrite, Cal-calcite.

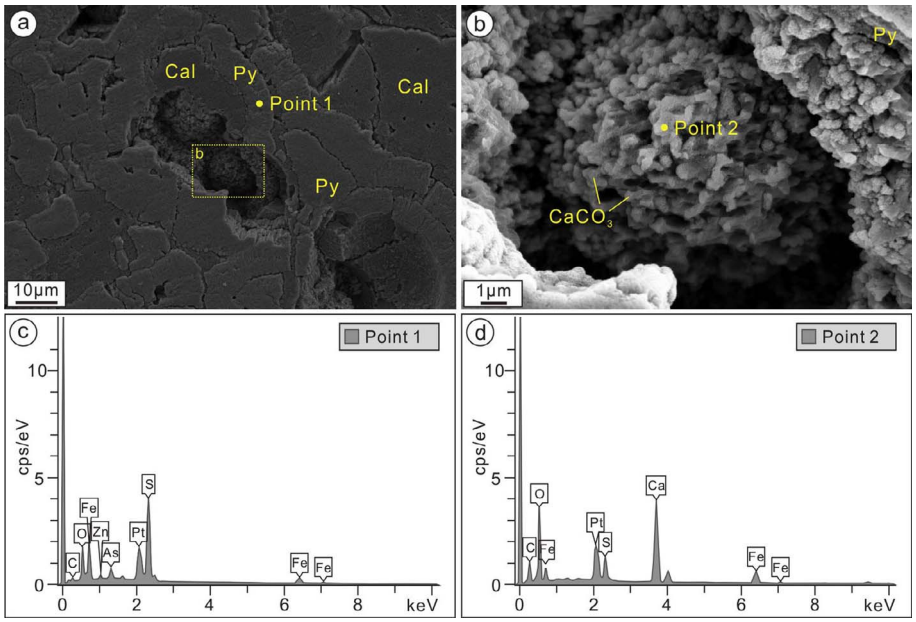

Fig. 6. FESEM photos and EDS analyses of bacteria fossils of calcite that occur with the colloidal sphalerite and pyrite (Sample JPMP-8 from sulfide ore in the Paopaping segment of the Jinding deposit). a. Assembly of potential micrococcus fossils of about 10 μm in diameter that are composed of calcite and related sulfide minerals; b. Magnification of a showing the calcite bacteria fossils forming an orbicular structure; c. EDS analysis of spot 1 in a; d. EDS analysis of spot 2 in b. Cal-calcite, Py-pyrite, Sp-sphalerite.

is similar to that found in the Engis and Ballinalack deposits with the internal spherical core having 2–3 layers of similar composition. Some Pb-Zn deposits in Belgium, Ireland, Poland and Austria also have similar sulfide mineral structures that have been interpreted to be the result of bacterial activity (Kucha, 1988; Kucha et al., 1990, 2001, 2005, 2010; Southam and Saunders, 2005). The Jinding Pb-Zn sulfide mineral structures described in Section 5.1 of this paper likely originated also as bacterial structures.

The galena and sphalerite plates, when seen in FESEM, consist of concentric spherical nuclei of galena and sphalerite with a diameter of 20–80 μm. The surface of the discontinuous sphalerite ring appears to consist of rough particles. On further magnification, the sphalerite

Table 1
S isotope composition of ore sulfides from the Jinding Zn–Pb deposit analyzed by SIMS.

No.	Segment	Point No.	Minerals	$^{34}S/^{32}S$	1σ (‰)	$\delta^{34}S$ (VCDT)	2σ (‰)
JJYS-12	Jiayashan	JJYS-12a	Sphalerite	4.325682	0.4	−9.5	0.6
		JJYS-12b	Sphalerite	4.324097	0.5	−9.7	0.6
		JJYS-12c	Sphalerite	4.303726	0.4	−14.5	0.6
		JJYS-12d	Sphalerite	4.313375	0.4	−12.3	0.6
JBC-7	Beichang	JBC-7a	Sphalerite	4.300668	0.4	−15.1	0.6
		JBC-7b	Sphalerite	4.281595	0.5	−19.6	0.6
		JBC-7c	Sphalerite	4.289725	0.4	−17.6	0.6
		JBC-7d	Sphalerite	4.286358	0.4	−18.5	0.6
		JBC-7e	Galena	4.335608	0.4	−33.5	0.6
		JBC-7f	Galena	4.338261	0.3	−32.9	0.6
		JBC-7g	Galena	4.32989	0.3	−34.9	0.6
JPMP-7	Paomaping	JPMP-7a	Sphalerite	4.290701	0.4	−17.5	0.6
		JPMP-7b	Sphalerite	4.287782	0.4	−18.1	0.6
		JPMP-7c	Sphalerite	4.29173	0.4	−17.3	0.6
		JPMP-7d	Pyrite	4.214577	0.3	−21.7	0.5
		JPMP-7e	Pyrite	4.216318	0.3	−21.6	0.5
		JPMP-7f	Pyrite	4.220004	0.3	−20.7	0.5
		JPMP-7g	Pyrite	4.204432	0.3	−24.3	0.5
		JPMP-7h	Pyrite	4.155106	0.3	−35.7	0.5
		JPMP-7i	Pyrite	4.212026	0.3	−22.5	0.5
JPMP-8	Paomaping	JPMP-8a	Sphalerite	4.309358	0.4	−13.2	0.6
		JPMP-8b	Sphalerite	4.296367	0.4	−16.3	0.6
		JPMP-8c	Sphalerite	4.301318	0.4	−14.9	0.6
		JPMP-8d	Pyrite	4.216515	0.3	−21.4	0.5
		JPMP-8e	Pyrite	4.217001	0.3	−21.3	0.5
		JPMP-8f	Pyrite	4.225646	0.3	−19.4	0.5
JFZS-8	Fengzishan	JFZS-8a	Pyrite	4.219362	0.4	−42.8	0.6
		JFZS-8b	Pyrite	4.226805	0.3	−41.1	0.7
		JFZS-8c	Pyrite	4.216046	0.3	−43.3	0.7
		JFZS-8d	Pyrite	4.224439	0.4	−41.5	0.7
		JFZS-8e	Galena	4.269055	0.4	−47.9	0.4
		JFZS-8f	Galena	4.266008	0.4	−48.6	0.4
		JFZS-8g	Galena	4.290957	0.4	−43	0.4

Note: This experiment was carried out on ion micoroprobe machine model CAMECA IMS-7F of SIMA laboratory in University of Manitoba, Canada.

assemblage actually consists of many tiny sphalerite microspheres, each with a diameter of about 200 nm. The sphalerite microspheres are connected to each other in a cluster by adhesive filaments of sphalerite nuclei. These plates have the morphological characteristics of bacterial colonies. In orbicular sphalerite from the Bleiberg deposit, we observed nanometer spheriods (10–90 nm) and bacterial filament structures by FESEM that can be interpreted to be the product of in situ metabolism by SRB. The micron-sized sphalerite spheres are composed of an assembly of sphalerite nanospheres, possibly from the replacement of bacterial colonies. This suggests the internal shape of the plate sphalerite crystallites, the galena assembly of nanospheres and the adhesion filaments all originated as bacteria in a secretion of extracellular substances (EPS) with subsequent sulfide (sphalerite) replacement to form the mineralized fossils in the ore.

FESEM examination shows the multicore gelatinous sphalerite-pyrite samples to be granular aggregates at a micron scale (Fig. 2g). The pyrite aggregates have a rough surface composed of numerous nanoscale pyrite spheres with a similar framboidal structure (Fig. 4c). Unlike the commonly seen spherical framboidal microcrystallites that usually have a cubic octahedral or pentagonal symmetry, the framboidal pyrite at Jinding consists of mostly orbicular nanometer aggregates of spherulites of ~200 nm in diameter. The observed morphologies share several similarities with the multicore gelatinous sphalerite-pyrite samples and the mineral microspheres that are found in biofilms of SRB (see Labrenz et al., 2000, Fig. 2). Labrenz et al. (2000) concluded that SRB in a low temperature environment can accelerate the formation of nanometer sphalerite and gather it into globular clusters with a biofilm morphology.

Pyrite in lead and zinc sulfide ore samples is often found in colloidal concentric rings and globular structures as pellets with a diameter of 20–40 μm (Fig. 5a). The pellets are composed of colloidal pyrite spheres of micro-nanometer size. The pellets in turn connect to each other to form a cluster (Fig. 5b and c). FESEM photos show pyrite filaments adhere to bind the pellets together (Fig. 5c). The colloidal pyrite microspheres have similar shape characteristics as the plate galena-sphalerite aggregates that also exhibit nanoscale sphalerite and filaments. They differ in that the galena-sphalerite pellets are larger and more dense, and the filaments between the tiny pyrite spheres are relatively smaller. Core observations of colloidal pyrite in shoaling- and sandstone-type uranium deposits exhibit crystalline uranium staphylococci that are very similar and considered to be formed by SRB (Min et al., 2005; Cai et al., 2007).

FESEM observations show sphalerite and pyrite nanospheres with associated with adhesive filaments that are also visible in symbiotic microsized calcite mineral aggregates (Fig. 6a). These aggregates are composed of numerous small spherical pelletized calcite clusters that are ~10 μm in diameter (Fig. 6b). These nanoscale pelletized minimers are also composed of calcite. Recent studies show that the sulfate-reducing bacteria can, when reducing sulfate, produce CO_2 by the oxidation of organic matter at the same time. The CO_2 in water and electricity generated from the production of HCO^{3-} can then react with Ca^{2+} to form calcite. When these processes occur in bacterial cells or in bacterial secreted extracellular polymers on a surface, the microorganisms wrap themselves in extracellular material to form petrochemical organisms that are preserved in situ (Stocks Fischer et al., 1999; Wang et al., 2013).

In general, the sulfide bacterial structures in the Jinding deposit are in single spheres with a diameter of about 200–500 nm that are slightly smaller than normal bacteria (0.5–2 μm). Usually the structure is subspherulitic and clustered in distribution with some filaments. This suggests that both the spheres and filaments are jointly produced by the bacteria to form the structure and the core of sulfide aggregates (Figs. 3–6). Morphologically the structures are similar in character to modern micrococci. Sometimes single fossil bacteria and adhesive filaments come together to form larger micron-sized orbicular clusters (Figs. 2–6) of mostly bacterial colonies (Toporski et al., 2002). EDS analysis of the bacterial fossils, adhesive filaments and calcite minerals indicate that they are composed of sphalerite, pyrite, etc. Thus the observed structures could either be primary sphalerite, pyrite and calcite, originally precipitated in bacterial cells and along adhesive filaments, or a later replacement or recrystallization of the original minerals (Love, 1957, 1962; Love and Zimmerman, 1961; Steinike, 1963; Massaad, 1974; Taylor, 1982; Stocks Fischer et al., 1999; Logan et al., 2001). The chondrules in the Jinding sulfide ore are slightly larger than most nano-sized bacterial fossils, but have similar characteristics. Most nanometer fossil bacteria in carbonate, sulfur, silicon oxide and clay are generally of only 50–200 nm in size, which is about one-tenth the diameter of common bacteria and one-thousandth of the volume. Compared to common bacteria, they are very similar in appearance but show obvious differences to most mineral particles because they can be spherical, rod-shaped, beads, etc., and are often part of dense colonies (Folk, 1993, 1996, 1999). Furthermore, most researchers believe that the mineral microspheres and their aggregates are associated with the bacterial biofilm nucleation effect (Labrenz et al., 2000; Riding, 2002; Labrenz and Banfield, 2004; Wang et al., 2013). Although biological processes can also produce similar fossil bacteria spheres, they usually have a wide range in size and nonuniformity (Liebig et al., 1996; Westall, 1999). The bacterial and biological spheres also differ in terms of sulfur isotope, biogenic minerals enrichment of light sulfur, etc (see below). Generally speaking, when fossil spheres and club-shaped fossil spheres are seen together, they are thought to be biogenic (Westall, 1999; Toporski et al., 2002). The nanospheres of Jinding sulfide ore minerals with linking filaments of mucoid bacterial extracellular polymeric substances (EPS) (Figs. 3c and d, 5c) suggest the potential for mineralization of bacteria cells or mineral microspherulites that were produced on a bacterial biofilm.

Bacterial fossils are common in many environments (Ehrlich and Newman, 2009) and they can be preserved by sulfate-reducing products such as pyrite, sphalerite, etc. Replacement of fossil bacteria by ancient SRB activity is evident in this study (Buick, 2001; Kucha et al., 2001; Shen and Schopf, 2004). Sulfate reducing bacteria (SRB) are generally anaerobic and found on the sea bottom, on land in polar environments and throughout hydrothermal systems (Widdel, 1988; Jørgensen et al., 1992; Sagemann et al., 1998). In general, suitable bacteria survive in temperatures from 0 to 80 °C (Machel, 2001). There are also some extreme thermophilic bacteria that can survive in temperatures as high as 121 °C (Kashefi and Lovley, 2003). At the appropriate temperature, SRB can get energy by the reduction of sulfate as an electron acceptor, by the oxidation of organic matter as an electron donor when accompanied by the release of H_2S and CO_2 (Madigan et al., 2010), and by the formation of biogenic material when the environment contains Ca^{2+} calcite. Thus reaction process can be simplified as

$$2CH_4 + Ca^{2+} + 2SO_4^{2-} + 2H^+ \rightarrow 2H_2\,S + CaCO_3 + 3H_2\,O + CO_2 \quad (1)$$

In Eq. (1), the CH_4 represents most hydrocarbons and other organic matter; $SO_4{}^{2-}$ represents soluble sulfate (gypsum and anhydrite, etc.); and, $CaCO_3$ represents calcite (Warren, 2000). When the H_2S, which was generated by this process, encounters Fe^{2+}, Zn^{2+} and Pb_{2+}, the H_2S quickly induces sulfide precipitation.

Sulfate reducing bacteria and its extracellular material can not only restore sulfate and generate a reducing H_2S (Rickard, 2012), they also can be used in the processing of polysaccharide substances when adsorbed on the surface of the biofilm with Fe^{2+}, Zn^{2+} and Ca^{2+} by changing the surrounding environment to provide ideal nucleation sites for mineral growth (Ferris et al., 1987; Large et al., 2001; Riding, 2002; Braissant et al., 2007; Wang et al., 2013). Sulfide minerals grow and precipitate on a cell surface or biological membrane surface where they can produce the intake of nutrients by the bacteria on the surface that cause the bacterial cells to die because of hunger. Thereafter the mineralization process continues to completely preserve the bacterial fossils in situ (Southam and Saunders, 2005) Further, the mineralization

continues by peripheral growth on the fossil SRB bacteria as shown in Fig. 2.

6.2. Sulfur isotopic composition

Generally, during the process of sulfate bacteria reduction, the lighter sulfur (^{32}S) tends to react faster than the heavier sulfur (^{34}S) because the weaker ^{32}S—O bonds is easier to break than the ^{34}S—O bond. Hence, the product H_2S is enriched in ^{32}S and depleted in ^{34}S, so that the value of the residual $\delta^{34}S$ sulfate will increase gradually as the reaction proceeds (Shen and Schopf, 2004; Seal, 2006). Therefore, a negative $\delta^{34}S$ value is generally deemed to be associated with SRB (Fallick et al., 2001; Southam et al., 2001; Kucha et al., 2001, 2005, 2010; Bawden et al., 2003; Schroll and Rantitsch, 2005).

The $\delta^{34}S$ values of sulfide at Jinding range from −48.6‰ to −9.5‰ with an average of −25.2‰ by SIMS analysis. The $\delta^{34}S$ value of sphalerite is between −19.6‰ and −9.5‰ with an average of −15.3‰ (n = 14), galena is between −48.6‰ and −32.9‰ with an average of −40.1‰ (n = 6) and pyrite is between −43.3‰ and −19.4‰ with an average of −29.0‰ (n = 13) (Table 1). Conversely, from the $\delta^{34}S$ values of the sulfate minerals in the Jinding dome (+6.3‰ to +21.7‰; Yin et al., 1990; Gao, 1991; Zhou and Zhou, 1992), we obtain a range of $\Delta_{SO4\text{-}sulfide}(=\delta^{34}S_{sulfate} - \delta^{34}S_{sulfide})$ between 15.8‰ and 70.3‰. Previous studies have shown that $\Delta_{SO4\text{-}sulfide}$ reaches a maximum of about 46‰ when produced by normal bacterial sulfate reduction (BSR) under laboratory conditions (Canfield, 2001; Fallick et al., 2001; Habicht and Canfield, 2001), whereas the fractionation of sulfides having bacteriogenic structures in the Jinding deposit ranges up to ~70‰ relative to the symbiotic sulfate. Such a large degree and wide range of fractionation indicates that the formation of the bacteriogenic structures is associated with SRB in the sulfide minerals and microspheres (Machel et al., 1995; McGowan et al., 2003; Carrillo-Rosúa et al., 2014). This suggests that disproportional fractionation of the bacteria may also be involved in the mineralization process except for BSR (Canfield, 2001; Fallick et al., 2001; Habicht and Canfield, 2001). Some research shows that single-step sulfate-reducing bacteria can produce nearly 75% of sulfur isotope fractionation in situ if the deposit was formed in the deep biosphere range (Wortmann et al., 2001). However, this does not conform to the subsurface environment of the Jinding dome.

In addition, the $\delta^{34}S_{VCDT}$ values of residual sulfate after the BSR process were heavier than the initial sulfate values of about 20–25‰ (Xue et al., 2015). The $\delta^{34}S$ values of the sulfate minerals associated with the Jinding metal sulfides varies from +6.3‰ to +21.7‰, which is similar to the $\delta^{34}S$ of Late Triassic Paleo-ocean sulfate (Yin et al., 1990; Gao, 1991; Zhou and Zhou, 1992). Therefore, the sulfate sulfur isotope characteristics of BSR in the Jinding deposit were created in a relatively open system with a sufficient supply of sulfate for the reaction system (Seal, 2006), which is consistent with the fact that there is a large amount of the gypsum in the Jinding deposit.

6.3. Bacterial reproduction and the formation mechanism of H_2S

The Jinding lead–zinc deposit is located in the northern part of the Lanping-Simao basin, which contains mainly Cenozoic clastic rocks, carbonate rocks and evaporites (Xue et al., 2004). The ore bodies are in the Yunlong and Jinxing formations. No magmatic rocks and almost no occurrences of hydrothermal alteration are found in either the overlying Eocene series and Quaternary system or in the underlying Sanhedong, Waluba, Maichuqing, Huakaizuozu, Nanxing, and Hutousi formations. Recent studies have shown that the lead–zinc mineralization was formed at a depth of ~1 km (Wen et al., 1995; Xue et al., 2002a, 2007a,c) in ancient reservoirs that contained plenty of organic matter prior to Zn-Pb mineralization (Xue et al., 2007c). Gypsum is found typically in continental evaporite strata and mineralized formations (Xue et al., 2006). These conditions show that the Jinding dome provided an epithermal environment rich in sulfate and organic matter that allowed the SRB to quickly multiply to complete the organic reduction of sulfate, and thus to produce H_2S rapidly and continually. When the BSR-produced H_2S then encounters elements such as Fe, Zn and Pb in abundance, precipitation takes place of large amounts of sulfide within the dome to form the common disseminated and massive mineral structures. Conversely, if mineralization takes place in the presence of SRB cells and extracellular material surfaces, then mineralized fossils will grow into an in situ sulfide bacterial structure. Thus, combining a micro-area of in situ S isotopes with H_2S, we believe that in situ BSR may have played a key role in the forming process of H_2S causing the Jinding Zn-Pb mineralization.

7. Conclusions

The ore of the Jinding deposit contains bacterial fossils with a diameter of 200–500 nm that are composed of sphalerite, galena, pyrite and calcite, either individually or in some combination. The fossils exhibit framboidal, botryoidal, rod-shaped, dendritic colloidal, metacolloidal, multinuclear-metacolloidal-zonal and plate-like structures.

In situ SIMS analyses of the bacterial fossils show that the sulfide minerals at Jinding have a wide range of $\delta^{34}S$ values from ~48.6‰ to ~9.5‰. Conversely the $\delta^{34}S$ values of sulfate minerals in the Lanping basin host rocks range from +6.3‰ to +21.7‰ that equates to a sulfer isotope fractionation range of +15.8‰ to +70.3‰, indicating that BSR produced the H_2S that precipitated the massive sulfides. The large difference in isotope fractionation values leads to the conclusion that the Jinding dome contained an oil and/or gas reservoir with a large amount of H_2S produced by BSR when the fertile lead and zinc-bearing hydrothermal fluids were introduced into the dome to precipitate the massive metal deposits.

Acknowledgements

This study was supported mainly by Grants to Xue from National Natural Science Foundation of China NSFC (41072069, 40772061). We sincerely thank Jinding Zinc Industry Co., Ltd for supporting the field geological survey and sample collection, and Dr. Dongjie and Tang Dr. Rong Liu for assistance during the experimental analysis.

References

Bai, J.F., Wang, C.H., Na, R.X., 1985. Geological characteristics of the Jinding lead-zinc deposit in Yunnan with a special discussion on its genesis. Miner. Deposits 4, 1–9 (in Chinese with English abstract).

Bawden, T.M., Einaudi, M.T., Bostick, B.C., Meibom, A., Wooden, J., Norby, J.W., Orobona, M.J.T., Chamberlain, C.P., 2003. Extreme 34S depletions in ZnS at the Mike gold deposit, Carlin Trend, Nevada: evidence for bacteriogenic supergene sphalerite. Geology 31, 913–916.

Bechtel, A., Shieh, Y.N., Pervaz, M., Püttmann, W., 1996. Biodegradation of hydrocarbons and biogeochemical sulfur cycling in the salt dome environment: inferences from sulfur isotope and organic geochemical investigations of the Bahloul Formation at the Bou Grine Zn/Pb ore deposit, Tunisia. Geochim. Cosmochim. Acta 60, 2833–2855.

Bechtel, A., Pervaz, M., Püttmann, W., 1998. Role of organic matter and sulphate-reducing bacteria for metal sulphide precipitation in the Bahloul Formation at the Bou Grine Zn/Pb deposit (Tunisia). Chem. Geol. 144, 1–21.

Braissant, O., Decho, A.W., Dupraz, C., Glunk, C., Przekop, K.M., Visscher, P.T., 2007. Exopolymeric substances of sulfate-reducing bacteria: interactions with calcium at alkaline pH and implication for formation of carbonate minerals. Geobiology 5, 401–411.

Buick, R., 2001. Life in the Archaean. In: Briggs, D.E.G., Crowther, P.R. (Eds.), Palaeobiology II. Blackwell, Oxford, pp. 13–21.

Cai, C.F., Dong, H.L., Li, H.T., Xiao, X.J., Ou, G.X., Zhang, C.M., 2007. Mineralogical and geochemical evidence for coupled bacterial uranium mineralization and hydrocarbon oxidation in the Shashagetai deposit, NW China. Chem. Geol. 236, 167–179.

Canfield, D.E., 2001. Biogeochemistry of sulfur isotopes. Rev. Mineral. Geochem. 43, 607–636.

Carrillo-Rosúa, J., Boyce, A.J., Morales-Ruano, S., Morata, D., Roberts, S., Munizaga, F., Moreno-Rodríguez, V., 2014. Extremely negative and inhomogeneous sulfur isotope signatures in Cretaceous Chilean manto-type Cu-(Ag) deposits, Coastal Range of central Chile. Ore Geol. Rev. 56, 13–24.

Chen, S.F., 1991. Geology and metal source of Jinding Stratabound Pb-Zn deposit, Lanping, Yunnan. Contribution to the Geology of the Qinghai-Xizang(Tibet). Plateau

21, 1–17 (in Chinese with English abstract).
Chen, S.F., 1992. A study on the isotope composition of S in the Jinding Pb-Zn deposit Lanping Yunnan. Geological Science and Technology Information. pp. 1–2 (in Chinese).
Chi, Guoxiang, Xue, Chunji, 2011. Abundance of CO2-rich fluid inclusions in a sedimentary basin-hosted Cu deposit at Jinman, Yunnan, China: implications for mineralization environment and classification of the deposit. Miner. Deposita 46, 365–380.
Ehrlich, H.L., Newman, D.K. (Eds.), 2009. Geomicrobiology CRC Press.
Fallick, A.E., Ashton, J.H., Boyce, A.J., Ellam, R.M., Russell, M.J., 2001. Bacteria were responsible for the magnitude of the world-class hydrothermal base metal sulfide orebody at Navan, Ireland. Econ. Geol. 96, 885–890.
Ferris, F.G., Fyfe, W.S., Beveridge, T.J., 1987. Bacteria as nucleation sites for authigenic minerals in a metal-contaminated lake sediment. Chem. Geol. 63, 225–232.
Folk, R.L., 1993. SEM imaging of bacteria and nannobacteria in carbonate sediments and rocks. J. Sediment. Res. 63 (5).
Folk, R.L., 1996. In defense of nannobacteria. Science (New York, NY) 274 (5291), 1288.
Folk, R.L., 1999. Nanobacteria and the precipitation of carbonate in unusual environments. Sed. Geol. 126 (1), 47–55.
Gao, G.L., 1991. Formation age and involved problems on anhydrite ore in Jinding lead-zinc ore area. Yunnan Geol. 10, 191–205 (In Chinese with English abstract).
Gao, Y.B., Xue, C.J., Zeng, R., 2008a. Forming mechanisms of H2S in the Jinding Pb-Zn deposit, Lanping Basin, Northwest Yunnan Province. J. Earth Sci. Environ. 30, 367–372 (in Chinese with English abstract).
Gao, Y.B., Xue, C.J., Zeng, R., 2008b. Geochemistry of organic matters in the Jinding zinc-lead deposit, Lanping Basin, Northwest Yunnan Province. Geochimica 37, 223–232 (in Chinese with English abstract).
Gustafson, L.B., Williams, N., 1981. Sediment-hosted stratiform deposits of copper, lead, and zinc. Econ. Geol. 75, 139–178.
Habicht, K.S., Canfield, D.E., 2001. Isotope fractionation by sulfate-reducing natural populations and the isotopic composition of sulfide in marine sediments. Geology 29, 555–558.
Hu, G.Y., Li, Y.H., Zeng, P.S., 2013. The role of halosalt in mineralization of the Jinding Zn-Pb deposit: evidence from Sulfur and Strontium isotopic compositions. Acta Geol. Sinica 87, 1694–1702 (in Chinese with English abstract).
Jørgensen, B.B., Isaksen, M.F., Jannasch, H.W., 1992. Bacterial sulfate reduction above 100°C in deep-sea hydrothermal vent sediments. Science 258, 1756–1757.
Kashefi, K., Lovley, D.R., 2003. Extending the upper temperature limit for life. Science 301, 934.
Kohn, M.J., Riciputi, L.R., Stakes, D., Orange, D.L., 1998. Sulfur isotope variability in biogenic pyrite: reflections of heterogeneous bacterial colonization? Am. Mineral. 83, 1454–1468.
Kucha, H., 1988. Biogenic and non-biogenic concentration of sulphur and metals in the carbonate-hosted Ballinalack Zn-Pb deposit, Ireland. Mineral. Petrol. 38, 171–187.
Kucha, H., Van der Biest, J., Viaene, W.A., 1990. Peloids in stratabound Zn-Pb deposits and their genetic importance. Miner. Deposita 25, 132–139.
Kucha, H., Schroll, E., Stumpfl, E.F., 2001. Direct Evidence for Bacterial Sulphur Reduction in Bleiberg-Type Deposits Mineral Deposits at the Beginning of the 21th Century. Swetz & Zeitlinger Publ., Lisse, pp. 149–152.
Kucha, H., Schroll, E., Stumpfl, E.F., 2005. Fossil sulphate-reducing bacteria in the Bleiberg lead-zinc deposit, Austria. Miner. Deposita 40, 123–126.
Kucha, H., Schroll, E., Raith, J.G., Halas, S., 2010. Microbial sphalerite formation in carbonate-hosted Zn-Pb ores, Bleiberg, Austria: micro-to nano-textural and sulfur isotope evidence. Econ. Geol. 105, 1005–1023.
Kyle, J.K., Li, N., 2002. Jinding: a giant tertiary sandstone-hosted Zn-Pb deposit, Yunnan, China. SEG Newslett. 50, 8–16.
Labrenz, M., Banfield, J.F., 2004. Sulfate-reducing bacteria-dominated biofilms that precipitate ZnS in a subsurface circumneutral-pH mine drainage system. Microb. Ecol. 47, 205–217.
Labrenz, M., Druschel, G.K., Thomsen-Ebert, T., Gilbert, B., Welch, S.A., Kemmer, K.M., Logan, G.A., Summons, R.E., De Stasio, G., Bond, P.L., Lai, B., Kelly, S.D., Banfield, J.F., 2000. Formation of sphalerite (ZnS) deposits in natural biofilms of sulfate-reducing bacteria. Science 290, 1744–1747.
Large, D.J., Fortey, N.J., Milodowski, A.E., Christy, A.G., Dodd, J., 2001. Petrographic observations of iron, copper, and zinc sulfides in freshwater canal sediment. J. Sediment. Res. 71, 61–69.
Liebig, K., Westall, F., Schmitz, M., 1996. A study of fossil microstructures from the Eocene messel formation using transmission electron microscopy with 3 figures in the text Neues Jahrbuch fur. Geol. Palaontol.-Monatshefte 4, 218–231.
Logan, G.A., Hinman, M.C., Walter, M.R., Summons, R.E., 2001. Biogeochemistry of the 1640 Ma McArthur River (HYC) lead-zinc ore and host sediments, Northern Territory, Australia. Geochim. Cosmochim. Acta 65, 2317–2336.
Love, L.G., 1957. Micro-organisms and the presence of syngenetic pyrite. Q. J. Geol. Soc. 113, 429–440.
Love, L.G., 1962. Biogenic primary sulfide of the Permian Kupferschiefer and Marl Slate. Econ. Geol. 57, 350–366.
Love, L.G., Zimmerman, D.O., 1961. Bedded pyrite and micro-organisms from the Mount Isa Shale. Econ. Geol. 56, 873–896.
Lü, B.X., Qian, X.G., 1999. A petrographic study on the hypogenic enclave in Cenozoic alkali volcanics and rich-alkali porphyry of west Yunnan. Yunnan Geol. 18 (2), 127–143 (in Chinese with English abstract).
Machel, H.G., 2001. Bacterial and thermochemical sulfate reduction in diagenetic settings–old and new insights. Sed. Geol. 140, 143–175.
Machel, H.G., Krouse, H.R., Sassen, R., 1995. Products and distinguishing criteria of bacterial and thermochemical sulfate reduction. Appl. Geochem. 10, 373–389.
Madigan, M.T., Martinko, J.M., Stahl, D.A., Clark, D.P., 2010. Brock biology of microorganisms-13th ed.
Marshall, C.P., Mackenzie, K.L., Chen, J., Oehler, D.Z., Logan, G.A., Walter, M.R., 2004. Microbes, organic matter and ore deposits. Microbiology Australia 25, 36–38.
Massaad, M., 1974. Framboidal pyrite in concretions. Miner. Deposita 9, 87–89.
McGowan, R.R., Roberts, S., Foster, R.P., Boyce, A.J., Coller, D., 2003. Origin of the copper-cobalt deposits of the Zambian Copperbelt: an epigenetic view from Nchanga. Geology 31, 497–500.
Min, M.Z., Xu, H.F., Chen, J., Fayek, M., 2005. Evidence of uranium biomineralization in sandstone-hosted roll-front uranium deposits, northwestern China. Ore Geol. Rev. 26, 198–206.
Rickard, D., 2012. Sulfidic Sediments and Sedimentary Rocks. Newnes.
Rickard, D.T., Zweifel, H., 1975. Genesis of Precambrian sulfide ores, Skellefte district, Sweden. Econ. Geol. 70, 255–274.
Riding, R., 2002. Microbial carbonates: the geological record of calcified bacterial-algal mats and biofilms. Sedimentology 47, 179–214.
Sagemann, J., Jørgensen, B.B., Greeff, O., 1998. Temperature dependence and rates of sulfate reduction in cold sediments of Svalbard. Arctic Ocean Geomicrobiol. J. 15, 85–100.
Schroll, E., Rantitsch, G., 2005. Sulphur isotope patterns from the Bleiberg deposit (Eastern Alps) and their implications for genetically affiliated lead-zinc deposits. Mineral. Petrol. 84, 1–18.
Scott, R.J., Meffre, S., Woodhead, J., Gilbert, S.E., Berry, R.F., Emsbo, P., 2009. Development of framboidal pyrite during diagenesis, low-grade regional metamorphism, and hydrothermal alteration. Econ. Geol. 104, 1143–1168.
Seal, R.R., 2006. Sulfur isotope geochemistry of sulfide minerals. Rev. Mineral. Geochem. 61, 633–677.
Shen, Y., Schopf, R., 2004. The antiquity of microbial sulfate reduction. Earth-Sci. Rev. 64, 243–272.
Shi, J.X., Yi, F.H., Wen, Q.D., 1983. The rock-ore characteristics and mineralization of Jinding lead-zinc deposit, Lanping. Yunnan Geol. 2, 179–195 (in Chinese with English abstract).
Southam, G., Saunders, J.A., 2005. The geomicrobiology of ore deposits. Econ. Geol. 100, 1067–1084.
Southam, G., Donald, R., Röstad, A., Brock, C., 2001. Pyrite discs in coal: evidence for fossilized bacterial colonies. Geology 29, 47–50.
Steinike, K., 1963. A further remark on biogenic sulfides; inorganic pyrite spheres. Econ. Geol. 58, 998–1000.
Stocks Fischer, S., Galinat, J.K., Bang, S.S., 1999. Microbiological precipitation of CaCO3. Soil Biol. Biochem. 31, 1563–1571.
Tang, Y.Y., Bi, X.W., Fayek, M., Wu, L.Y., Zou, Z.C., Feng, C.X., Wang, X.S., 2014. Microscale sulfur isotopic compositions of sulfide minerals from the Jinding Zn-Pb deposit, Yunnan Province, southwest China. Gondwana Res. 26, 594–607.
Taylor, G.R., 1982. A mechanism for framboid formation as illustrated by a volcanic exhalative sediment. Miner. Deposita 17, 23–36.
Toporski, J.K.W., Steele, A., Westall, F., Avci, R., Martill, D.M., McKay, D.S., 2002. Morphologic and spectral investigation of exceptionally well-preserved bacterial biofilms from the Oligocene Enspel formation, Germany. Geochim. Cosmochim. Acta 66 (10), 1773–1791.
Wacey, D., Kilburn, M.R., Saunders, M., Cliff, J.B., Kong, C., Liu, A.G., Matthews, J.J., Brasier, M.D., 2015. Uncovering framboidal pyrite biogenicity using nano-scale CNorg mapping. Geology 43, 27–30.
Wang, H.M., Wu, X.P., Qiu, X., Liu, D., 2013. Microbially induced carbonate precipitation: a review. Microbiology China 40, 180–189 (in Chinese with English abstract).
Warren, J.K., 2000. Evaporites, brines and base metals: low-temperature ore emplacement controlled by evaporite diagenesis. Aust. J. Earth Sci. 47, 179–208.
Watson, J.H.P., Cressey, B.A., Roberts, A.P., Ellwood, D.C., Charnock, J.M., Soper, A.K., 2000. Structural and magnetic studies on heavy-metal-adsorbing iron sulphide nanoparticles produced by sulphate-reducing bacteria. J. Magn. Magn. Mater. 214, 13–30.
Wen, C.Q., Cai, J.M., Liu, W.Z., Qin, G.J., Chen, S.F., 1995. Geochemical characteristics of fluid inclusions in the Jinding lead-zinc deposit, Yunnan. China J. Miner. Pet. 15, 78–84 (in Chinese with English abstract).
Westall, F., 1999. The nature of fossil bacteria: a guide to the search for extraterrestrial life. J. Geophys. Res. 104 (E7), 16437–16451.
Widdel, F., 1988. Microbiology and ecology of sulfate-and sulfur-reducing bacteria. Biol. Anaerobic Microorganisms 469–585.
Wortmann, U.G., Bernasconi, S.M., Böttcher, M.E., 2001. Hypersulfidic deep biosphere indicates extreme sulfur isotope fractionation during single-step microbial sulfate reduction. Geology 29 (7), 647–650.
Xue, C.J., Chen, Y.C., Yang, J.M., Wang, D.H., Yang, W.G., Yang, Q.B., 2002a. Analysis of ore-forming background and tectonic system of Lanping Basin, Western Yunnan Province. Miner. Deposits 21 (1), 11–23 (in Chinese with English abstract).
Xue, C.J., Chen, Y.C., Yang, J.M., Wang, D.H., 2002b. Jinding Pb-Zn deposit: geology and geochemistry. Miner. Deposits 21 (3), 270–277 (in Chinese with English abstract).
Xue, C.J., Chen, Y.C., Yang, J.M., 2003. Geology and isotopic composition of helium, neon, xenon and metallogenic age of the Jinding and Baiyangping ore deposits, northwest Yunnan, China. Sci. China (Series D) 46 (8), 789–800.
Xue, C.J., Liu, S.W., Chen, Y.C., Zeng, R., Zhao, S.H., 2004. Giant mineral deposits and their geodynamics setting in the Lanping Basin, Yunnan, China. Acta Geol. Sin. 78 (2), 368–374.
Xue, C.J., Chi, G.X., Chen, Y.C., Wang, D.H., Qing, H.R., 2006. Two fluid systems in the Lanping basin, Yunnan, China-their interaction and implications for mineralization. J. Geochem. Explor. 89, 436–439.
Xue, C.J., Zeng, R., Liu, S.W., Chi, G.X., Qing, H.R., Chen, Y.C., Yang, J.M., Wang, D.H., 2007a. Geologic, fluid inclusion and isotopic characteristics of the Jinding Zn-Pb deposit, western Yunnan, South China: a review. Ore Geol. Rev. 31, 337–359.

Xue, C.J., Gao, Y.B., Zeng, R., Chi, G.X., Qing, H.R., 2007b. Organic petrography and geochemistry of the giant Jinding deposit, Lanping basin, northwestern Yunnan, China. Acta Petrol. Sin. 23, 2889–2900 (in Chinese with English abstract).
Xue, C.J., Gao, Y.B., Zeng, R., Chi, G.X., 2007c. The genetic model of mineralization of the giant Jinding Pb-Zn deposit, north-western Yunnan. Bull. Mineral. Petrol. Geochem. (z1), 334–336 (in Chinese).
Xue, C.J., Gao, Y.B., Chi, G.X., David, L.L., 2009. Possible former oil-gas reservoir in the giant Jinding Pb-Zn deposit, Lanping, NW-Yunnan: the role in the ore accumulation. J. Earth Sci. Environ. 31, 221–229 (in Chinese with English abstract).
Xue, C.J., Chi, G.X., Xue, W., 2010. Interaction of two fluid systems in the formation of sandstone-hosted uranium deposits in the Ordos Basin: geochemical evidence and hydrodynamic modeling. J. Geochem. Explor. 106, 226–235.
Xue, C.J., Chi, G.X., Li, Z.D., Dong, X.F., 2014. Geology, geochemistry and genesis of the Cretaceous and Paleocene sandstone- and conglomerate-hosted Uragen Zn–Pb deposit, Xinjiang, China: A review. Ore Geol. Rev. 63, 328–342.
Xue, C.J., Chi, G.X., Fayek, M., et al., 2015. Micro-textures and in situ sulfur isotopic analysis of spheroidal and zonal sulfides in the giant Jinding Zn-Pb deposit, Yunnan, China: implications for biogenic processes. J. Asian Earth Sci. 103 (1), 288–304.
Yaxiaer, Y., Xue, C.J., Symons, D., 2017. Paleomagnetic age and tectonic constraints on the genesis of the giant Jinding Zn-Pb deposit, Yunnan, China. Miner. Deposita. http://dx.doi.org/10.1007/s00126-017-0733-9.
YBGMR (Yunnan Bureau Geology & Mineral Resources) (1990) Regional Geology of Yunnan Province Beijing: Geological Publishing House, 1–77 (in Chinese).
Yin, H.H., Fan, W.M., Lin, G., 1990. Deep processes and mantle-crust compound mineralization in the evolution of the Lanping-Simao Mesozoic-Cenozoic diwa basin in western Yunnan, China. Geotectonica Metall. 14, 113–124 (in Chinese with English abstract).
Zhou, W.Q., Zhou, Q.L., 1992. A study on the isotope composition of Pb and S in the Lanping Pb-Zn deposit, Yunnan Province. Geochemica 2, 141–148 (in Chinese with English abstract).
Zhu, S.Q., Qin, G.J., Wen, C.Q., Chen, S.F., 2000. Jinding: a giant Zn-Pb deposit in continental clastic rock. In: Tu, GZ, Super large ore deposits in China Beijing: Science Press 65–86 (in Chinese).